**Current Biology, Volume *30***

## Supplemental Information

# A Neural Representation of Naturalistic Motion-Guided Behavior in the Zebrafish Brain

**Tugce Yildizoglu, Clemens Riegler, James E. Fitzgerald, and Ruben Portugues**

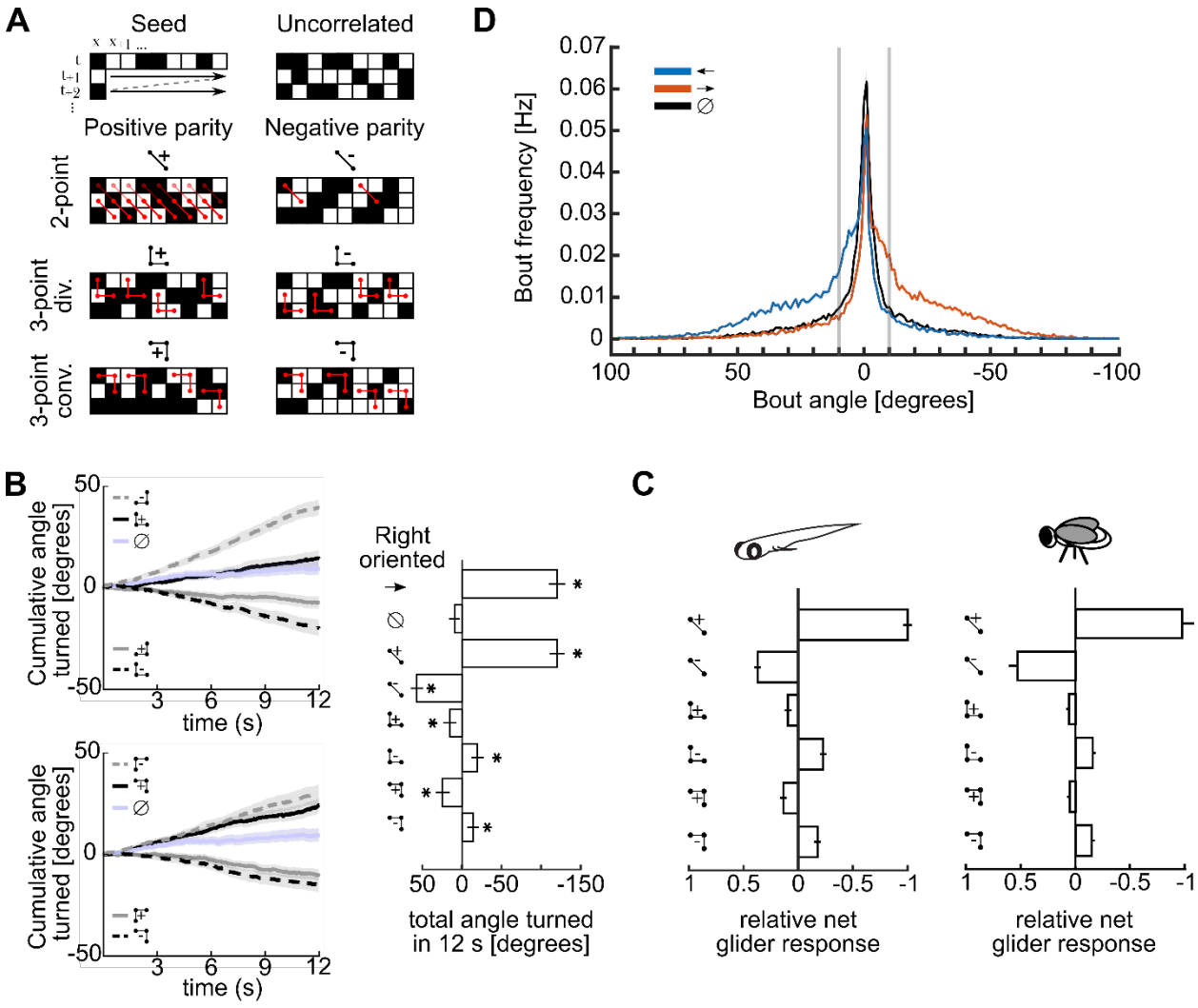


**Figure S1. Glider stimulus construction and the behavior they elicit, Related to Figure 2 and STAR Methods.** A) Construction of glider stimuli. Modified from [S1]. Generation of all stimuli began with a seed row and column, with right oriented stimuli seeded by the first column and left oriented stimuli seeded by the last column. The full spacetime map was then filled in one row at a time according to the correlation structure defining the update rule (see also STAR Methods). Example pixel configurations are shown in red for each right oriented glider pattern. Note that the product of any set of pixels connected by red links is consistent with the defining correlation of the stimulus. B) Fish-averaged mean turning responses quantified as the cumulative angle turned (N = 120 fish). Shaded error bars are SEM. Positive angles denote leftwards turns. Fish

responded direction selectively to diverging 3-point glider stimuli (top left) and converging 3-point glider stimuli (bottom left). Total angle turned during the complete 12 second trial for each non-directional or right oriented stimulus (right). Responses to all glider stimuli were significantly different from uncorrelated stimulus responses (all $p<0.01$, Wilcoxon test). Note that the direction of every glider response depended on the parity (correlation sign) of the glider. C) Net glider responses (right oriented stimulus response minus left oriented stimulus response), magnitudes relative to the net 2-point positive response, in larval zebrafish (left) and Drosophila (right, adapted from [S1]). Right oriented glider patterns are shown to signify each stimulus pair. Error bars are standard errors of the mean. D) Bout frequency histograms of bout angles (1 degree bins) averaged over all larvae for the uncorrelated stimulus and leftward and rightward drifting gratings. Grey lines are the threshold values separating right turns, forward swims, and left turns (e.g. Figure 2D).

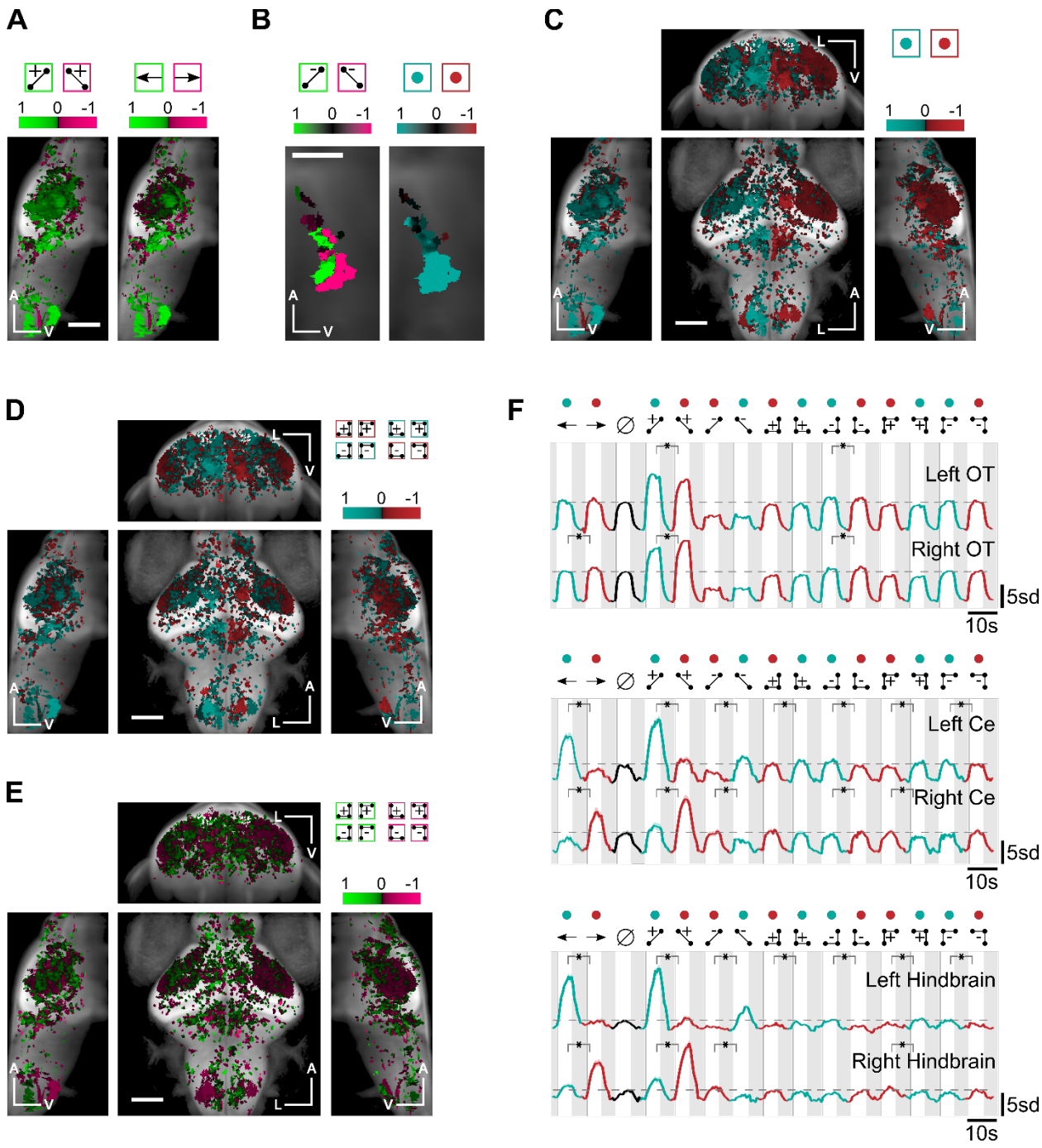


**Figure S2. Responses to diverse directional motion stimuli across the whole brain, Related to Figure 3.** A) Left sagittal projections (left of quartet) of the whole-brain direction-selectivity maps for positive 2-point gliders and drifting sine gratings. Data are presented according the same conventions of Figure 3C, D. B) Left sagittal projections omitted from the maps in Figure 3E, F. C) Whole-brain direction selectivity maps of ROIs across all stimuli driving left turning (green)

versus right turning (red). D) Whole-brain direction selectivity maps for 3-point glider stimuli driving left turning (green) versus right turning (red). E) Whole-brain direction selectivity maps for left oriented (green) versus right oriented (magenta) 3-point glider stimuli. Direction-selectivity with this index was weak. F) Mean z-scored fluorescence responses of ROIs in the left versus right Optic Tectum (OT), Cerebellum (Ce) and Hindbrain. Shaded error bars represent SEM. Green and red colored dots signify visual stimuli driving left turning and right turning, respectively. Horizontal dashed lines mark the peak average responses during the uncorrelated stimulus presentation. Asterisks indicate that all comparisons were significant at the $p = 0.01$ level (Wilcoxon test).

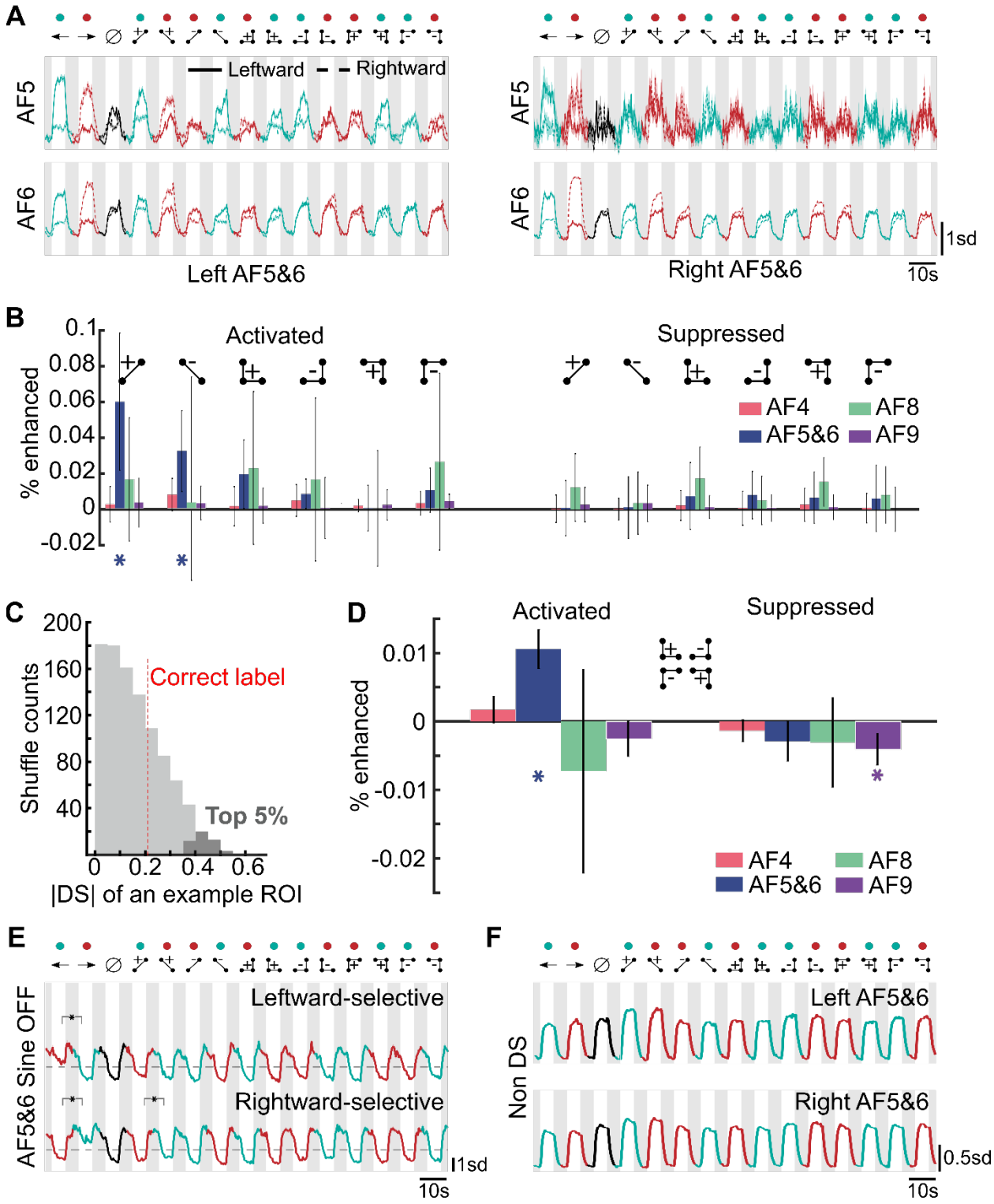


**Figure S3. Response properties of retinal ganglion cell ROIs to directional stimuli, Related to Figure 4.** A) Mean fluorescence traces of leftward (solid curves) and rightward (dashed curves) direction selective activated ROIs, shown separately for left AF5, left AF6, right AF5, and right AF6. The observed patterns largely matched those when AF5 and AF6 were merged into AF5&6

(Figure 4G), but we did not observe many direction selective ROIs in right AF5. Direction selectivity was assessed using ROI responses to drifting gratings alone. Shaded regions represent SEMs in this and subsequent panels. B) Assessment of direction selectivity for all individual stimulus pairs (STAR Methods). Note that the number of direction selective ROIs was above chance levels only for activated AF5&6 ROIs responding to positive 2-point and negative 2-point stimuli. Symbols for the left oriented stimuli are shown for representation purposes only, as both left- and right-oriented stimuli are used in the calculation. Error bars represent estimated 95% confidence intervals. C) The shuffle test was modified to pool ROIs responses across all 3-point glider stimuli (STAR Methods). As it would be very computationally heavy to account for every possible combination of 8 different 3-point stimuli labels, we picked a random sample of 999 shuffled labels and identified the specific ROI as direction selective if its correct label appears in the top 5% among 1000. D) This shuffle test shows that the number of direction selective ROIs was only above chance levels in the activated ROI population in AF5&6. E) Although AF5&6 had a statistically significant population of suppressed direction selective ROIs, this direction selectivity did not generalize to other stimuli. F) Mean fluorescence traces of non-direction-selective ROIs in left and right AF5&6.

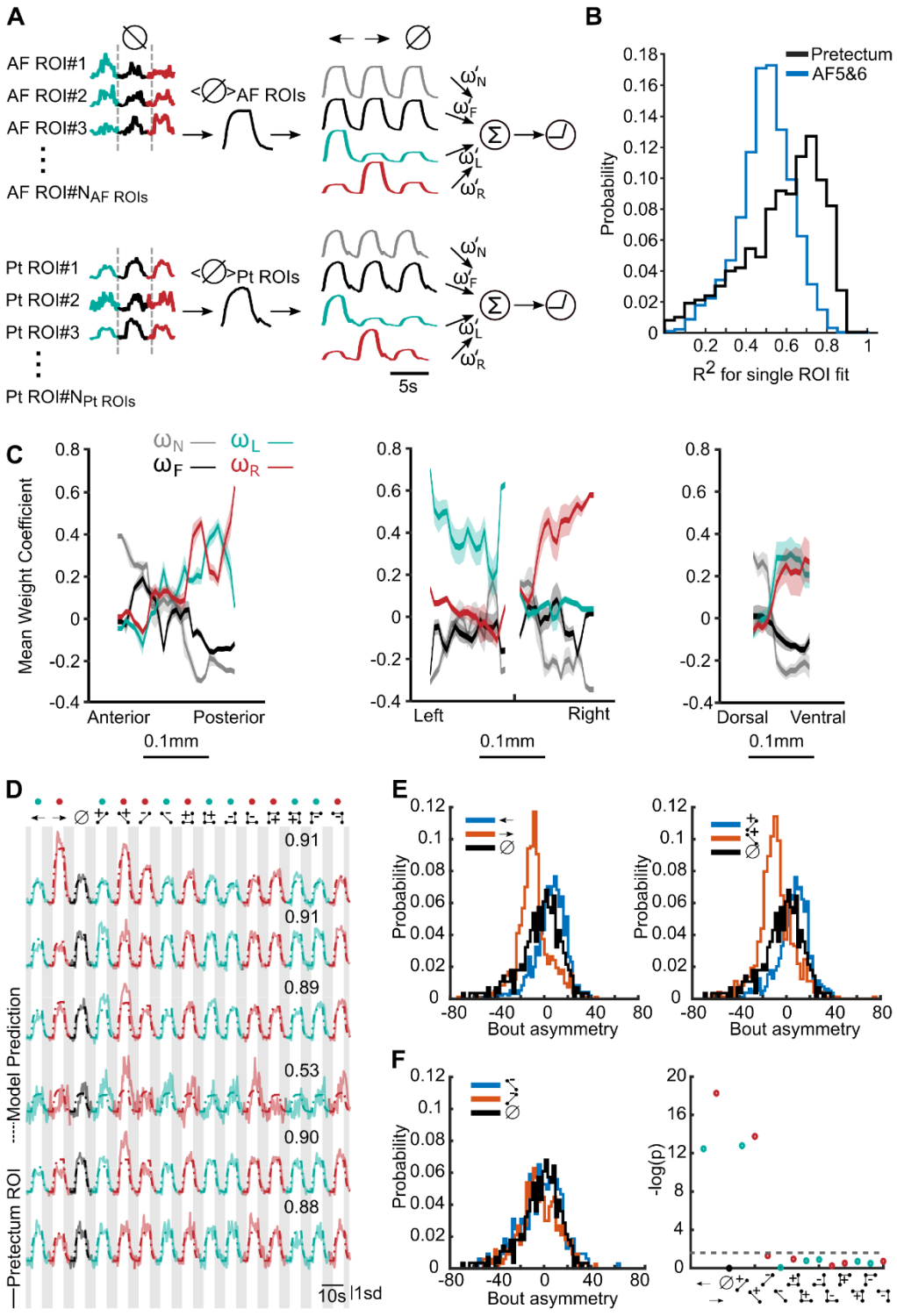


**Figure S4. Additional quantification of how behavioral patterns structure visual responses, Related to Figure 5.** A) Schematic of alternate model architecture in which mean fluorescence traces of AF5&6 and pretectum ROIs to uncorrelated stimulus were used to generate the

behavioral regressors (STAR Methods). We fit the model parameters with methods similar to the model with exponentially convolved behavioral regressors (STAR Methods, Figure 5A). B) Distribution of R-squared values for all ROIs. With the alternate regressors, the fraction of variance explained in the case of the AF5&6 responses fitted model was still shifted towards smaller values compared to pretectum case. C) Means of the weight coefficients mapped in Figure 5E across three anatomical axes. Shaded regions indicate SEM. D) Extension of Figure 5D to show six more example traces for individual pretectal ROIs alongside the associated model fits and R-squared values. E) We used a bout asymmetry index to detect directional behavior in head-embedded zebrafish (STAR Methods). The analysis revealed that head-embedded zebrafish exhibited directional behavior to drifting gratings (left) and positive 2-point glider stimuli (right). Positive values of bout asymmetry correspond to leftward turns. F) Head-embedded zebrafish did not exhibit directional behavior to negative 2-point glider stimuli (left), even though these stimuli drove strong fluorescence responses in the pretectum (Figure 3E, 3G, 5D, S2B, S4D). This shows that pretectal responses fail to predict moment-to-moment behavioral variability. Among all stimulus conditions, we found that only sine gratings and positive 2-point glider stimuli elicited bout asymmetry indices that significantly differed from behavior in response to uncorrelated noise (right, p-values from two-sample Kolmogorov-Smirnov test). The dashed line denotes the $p = 0.05$ significance level.

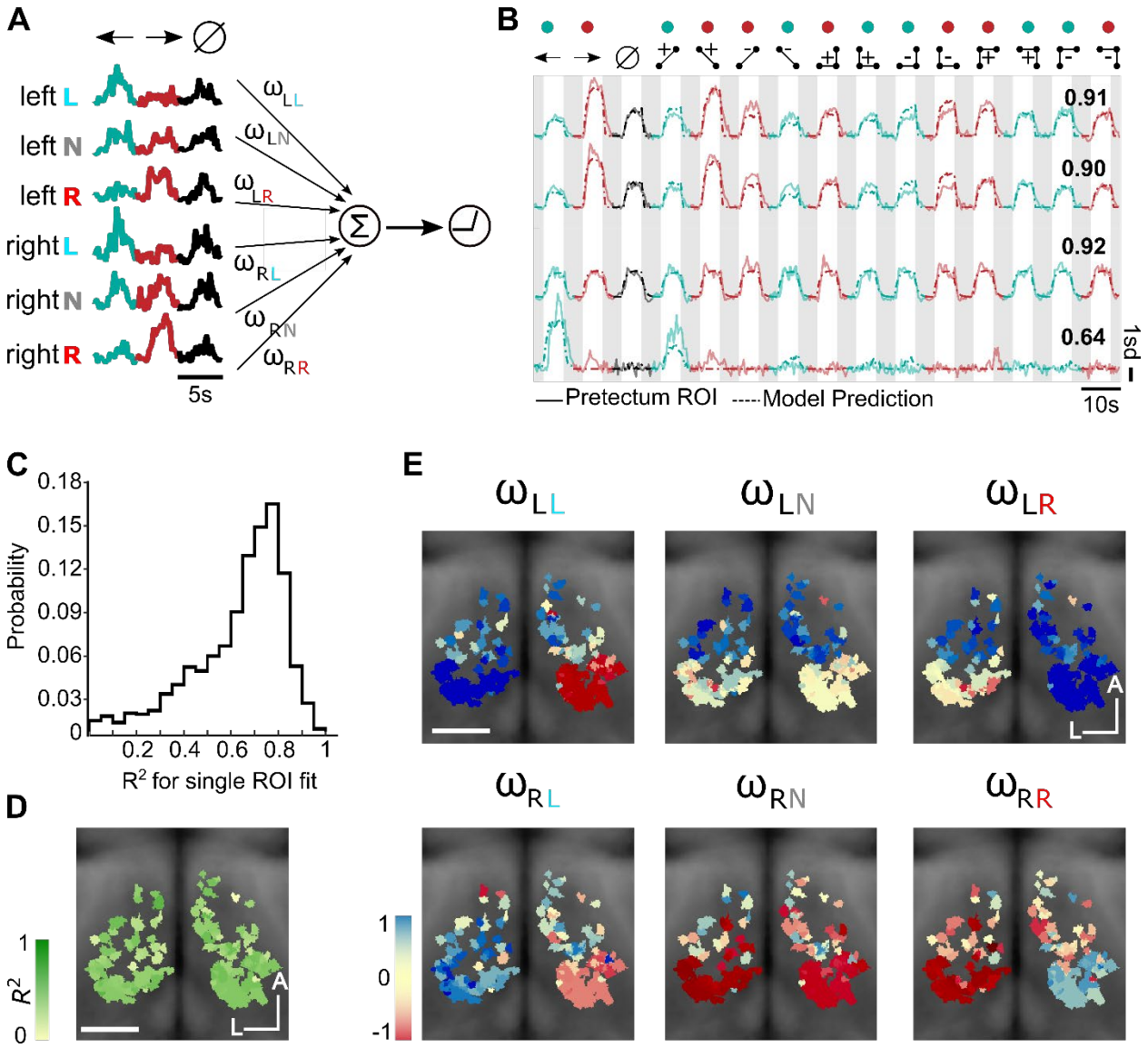


**Figure S5. Alternative model that explains the pretectal responses in terms of the responses in AF5&6, Related to Figure 5.** A) Schematic of alternate model architecture in which mean fluorescence traces of leftward, rightward and non-directional units in left and right AF5&6 are used as regressors (STAR Methods). We fit the model parameters with methods similar to the model with behavioral regressors. B) Example traces for four ROIs, together with the model predictions and R-squared values. C) Distribution of R-squared values (variance explained by model) for all ROIs. D) Coronal projection of R-squared map. A and L indicates the anterior-posterior left-right axes. Scale bar 0.1mm. E) Coronal projection maps of the weights of the six retinal regressors used in the model. Leftward (rightward) selective regressors from both left and right AF5&6 contributed to model prediction in left (right) pretectum. Scale bar 0.05 mm.

## SUPPLEMANTAL REFERENCES

S1. Clark, D.A., Fitzgerald, J.E., Ales, J.M., Gohl, D.M., Silies, M.A., Norcia, A.M., and Clandinin, T.R. (2014). Flies and humans share a motion estimation strategy that exploits natural scene statistics. Nat. Neurosci. *17*, 296–303.